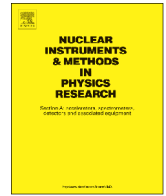




ELSEVIER

Contents lists available at ScienceDirect

# Nuclear Instruments and Methods in Physics Research A

journal homepage: [www.elsevier.com/locate/nima](http://www.elsevier.com/locate/nima)

## Electromagnetic Simulation and Design of a Novel Waveguide RF Wien Filter for Electric Dipole Moment Measurements of Protons and Deuterons



J. Slim<sup>a</sup>, R. Gebel<sup>b</sup>, D. Heberling<sup>a,c</sup>, F. Hinder<sup>b,d</sup>, D. Hölscher<sup>a</sup>, A. Lehrach<sup>b,c,d</sup>, B. Lorentz<sup>b</sup>, S. Mey<sup>b,d</sup>, A. Nass<sup>b</sup>, F. Rathmann<sup>b,\*</sup>, L. Reifferscheidt<sup>e</sup>, H. Soltner<sup>e</sup>, H. Straatmann<sup>e</sup>, F. Trinkel<sup>b,d</sup>, J. Wolters<sup>e</sup>

<sup>a</sup> Institute of High-Frequency Technology, RWTH Aachen University, 52074 Aachen, Germany

<sup>b</sup> Institute of Nuclear Physics (IKP), Forschungszentrum Jülich, 52428 Jülich, Germany

<sup>c</sup> JARA-FAME (Forces and Matter Experiments), Forschungszentrum Jülich and RWTH Aachen University, 52056 Aachen, Germany

<sup>d</sup> III. Physikalisches Institut B, RWTH Aachen University, 52074 Aachen, Germany

<sup>e</sup> Central Institute of Engineering and Analytics (ZEA), Forschungszentrum Jülich, 52428 Jülich, Germany

### ARTICLE INFO

#### Article history:

Received 4 March 2016

Received in revised form

29 April 2016

Accepted 4 May 2016

Available online 6 May 2016

#### Keywords:

Wien filter

Parallel-plates waveguide

Homogeneous electromagnetic field

Lorentz force compensation

### ABSTRACT

The conventional Wien filter is a device with orthogonal static magnetic and electric fields, often used for velocity separation of charged particles. Here we describe the electromagnetic design calculations for a novel waveguide RF Wien filter that will be employed to solely manipulate the spins of protons or deuterons at frequencies of about 0.1–2 MHz at the COoler SYNchrotron COSY at Jülich. The device will be used in a future experiment that aims at measuring the proton and deuteron electric dipole moments, which are expected to be very small. Their determination, however, would have a huge impact on our understanding of the universe.

© 2016 Elsevier B.V. All rights reserved.

### 1. Introduction

Recently, the use of a Wien filter operated at radio frequency (RF) has been proposed as a tool to search for electric dipole moments (EDMs) of protons and deuterons in storage rings [1,2]. The occurrence of EDMs of elementary particles is intimately connected to the matter–antimatter asymmetry observed in the universe [3], which the Standard Model of elementary particle physics fails to describe. A non-zero EDM measurement would point to new physics beyond the Standard Model [4].

A Wien filter provides orthogonal electric and magnetic fields, usually generated by a parallel-plate capacitor and encircling coils, such that the Lorentz force for charged particles traveling with a specific velocity orthogonal to both fields vanishes [5]. This principle has found widespread applications not only in mass spectrometers, but also in electron microscopes and ion optics [6]. A few reports have been dedicated to its use in accelerator facilities, but most of them describe static Wien filters [7,8]. The electric and

magnetic fields of an RF Wien filter can be used to manipulate the spins of particles in a storage ring, and, as shown in [1,2], open up the possibility for a measurement of the EDMs of protons and deuterons.

The objective of the present publication is to describe the design of a novel waveguide RF Wien filter for the search for the EDMs of protons and deuterons at COSY [9,10], pursued by the JEDI collaboration.<sup>1</sup> The fact that proton and deuteron EDMs are expected to be very small calls for precise design and manufacturing. We must admit that the spin-tracking tools required to provide specifications for the design of the RF Wien filter have not yet been fully developed. Recently, spin-tracking studies with an *ideal* RF Wien filter were carried out [11,12], but these do not yet take into account a number of important systematic effects, such as fringe fields, unwanted field components, positioning errors, and non-vanishing Lorentz forces. Therefore, an approach was adopted here to try to realize the best possible device based on state-of-the-art technologies.

\* Corresponding author.

<sup>1</sup> JEDI collaboration <http://collaborations.fz-juelich.de/ikp/jedi>.

A prototype RF Wien filter, based on an already existing RF dipole with radial magnetic field [13,14], was recently developed and used at COSY. (The use of RF dipoles and solenoids to manipulate stored polarized beams is discussed in [15].) The RF dipole was equipped with horizontal electric field plates in order to provide an RF Wien filter configuration with vertical electric and horizontal magnetic field [16,17]. The RF electromagnetic field was generated using two coupled resonators; one that generates the electric field and another one that generates the magnetic field. The approach of using separate systems to generate electric and magnetic fields, however, neglects the inherent coupling between these fields. Therefore, the approach described here, is based on a novel waveguide system where by design the orthogonality between electric and magnetic fields is accomplished.

The paper is organized as follows:

- **Section 2** describes the mechanical design of the RF Wien filter. The parallel-plates waveguide and its mechanical structure are described in **Section 2.1**, the driving circuit in **Section 2.2**. The results of the electromagnetic field simulations, the Lorentz force compensation, and the optimization of the electric and magnetic field homogeneity by shaping the electrodes is discussed in **Section 2.3**.
- **Section 3** describes the beam dynamics simulations. A Monte Carlo simulation was carried out in order to quantify the unwanted field components of the RF Wien filter with a realistic phase-space distribution of the beam. A comparison of the prototype RF Wien filter [16,17] and the waveguide RF Wien filter is given in **Section 3.3**.
- **Section 4** presents results of thermal simulations based on the power losses in the different materials of the device.

## 2. Design

### 2.1. Waveguide design

The RF Wien filter shall be operated at frequencies of about 100 kHz to 2 MHz. The maximum acceptable length for the vacuum vessel, given by space restrictions at COSY, is 870 mm, which corresponds to approximately 1/300 of the length of the electromagnetic wave (at 1 MHz). The transverse electromagnetic (TEM) mode of a parallel-plate waveguide fulfills the requirement of orthogonal electric and magnetic fields.

In order to maintain an overall vanishing Lorentz force, and to provide minimal unwanted field components, it is *a priori* not clear whether a small or a large beam size is advantageous. Within the COSY ring, the PAX low- $\beta$  section [10] offers the possibility to vary the beam size by about a factor of three, therefore the RF Wien filter will be installed at this location.

The design calculations for the waveguide RF Wien filter were carried out using a full-wave simulation with CST Microwave Studio,<sup>2</sup> and the electric and magnetic fields were modeled with an accuracy of  $10^{-6}$ . Because of the high expectations on field homogeneity, an approach was adopted that allows one to calculate the electric and magnetic fields without additional assumptions, such as quasi-static approximations or the like.<sup>3,4,5</sup>

<sup>2</sup> CST – Computer Simulation Technology AG, Darmstadt, Germany, <http://www.cst.com>.

<sup>3</sup> Each simulation required up to 12 h of computing time on a 4-T C2075 GPU cluster, with 2 six-core Xeon E5 processors and a RAM capacity of 94 GB.

<sup>4</sup> Nvidia Corporation, Santa Clara, California, USA, <http://www.nvidia.com/obj/ject/tesla-workstations.html>.

<sup>5</sup> Intel Corporation, Santa Clara, California, USA, <http://www.intel.com/content/www/us/en/processors/xeon/xeon-processor-e5-family.html>.

The system comprises a power source, a parallel plate waveguide and a load. The plates are fed on their front and rear sides by an RF current, which distributes on the surfaces, thereby generating the required electromagnetic field in the enclosed space. Deviations from the ideal orthogonality and homogeneity of the fields are due to the finite size of the plates and their limited conductivities.

The intended working frequencies of the RF Wien filter are calculated according to

$$f_{\text{RF}} = f_{\text{rev}} |k + \gamma G|, \quad k \in \mathbb{Z} \quad (1)$$

where  $k$  is the harmonic number,  $G$  the gyromagnetic anomaly,  $\gamma G$  the spin tune [18], and  $f_{\text{rev}}$  the revolution frequency. With respect to the search for the EDMs of deuterons and protons, experiments at a number of harmonics shall be carried out for systematic reasons. **Table 1** summarizes the resonance frequencies for deuterons at a momentum of 970 MeV/c and for protons at 520 MeV/c, for which electron-cooled beams with compensated cooler solenoid are available at COSY. As indicated in **Table 1** for deuterons (protons), five (four) harmonics are in the operating frequency range of 100 kHz to 2 MHz. In the following, we restrict the discussion to deuterons at a momentum of 970 MeV/c.

The Lorentz force is given by

$$\vec{F}_L = q \left( \vec{E} + \vec{v} \times \vec{B} \right), \quad (2)$$

where  $q$  is the charge of the particle,  $\vec{v} = c(0, 0, \beta)$  is the velocity vector,  $\vec{E} = (E_x, E_y, E_z)$  and  $\vec{B} = \mu_0(H_x, H_y, H_z)$  denote the components of the electric and magnetic fields, and  $\mu_0$  the vacuum permeability. For a vanishing Lorentz force  $\vec{F}_L = 0$ , the required field quotient  $Z_q$  is determined, which yields

$$\begin{aligned} E_x &= -c \cdot \beta \cdot \mu_0 \cdot H_y, \\ Z_q &= -\frac{E_x}{H_y} = c \cdot \beta \cdot \mu_0 \approx 173 \, \Omega. \end{aligned} \quad (3)$$

**Fig. 1** shows a cross section of the parallel-plates waveguide RF Wien filter. The axis of the waveguide points along the beam direction ( $z$ ). The width of the plates is 182 mm, and they are separated by 100 mm along the  $x$ -direction. This setup ensures that during the EDM studies at COSY, the main component of the electric field ( $E_x$ ) points radially inwards in the  $-x$ -direction, and the main component of the magnetic field ( $H_y$ ) upwards in the  $y$ -direction with respect to the stored beam. The system is placed inside a cylindrical vacuum vessel. The electrodes are surrounded by ferrite blocks made of CMD5005.<sup>6</sup> The copper electrodes are shaped in order to improve the homogeneity of the electric and magnetic fields and to minimize the Lorentz force, as explained in detail in **Section 2.3**.

A sophisticated support structure, shown in **Fig. 2**, was designed to ensure a high degree of rigidity, precision alignment and most importantly, low distortion of the generated electromagnetic field. The electrodes are made from double T-shaped copper plates for better stiffness and stability. They are mounted with 12 stainless-steel screws on the main support structure of the electrodes. An inner stainless-steel tube is used to hold, align and mount the structure with high precision ( $\approx 10 \, \mu\text{m}$ ).

The angular position of the RF Wien filter with respect to the beam axis can be chosen to allow for a rotation of the field direction by  $90^\circ$  with an angular precision of  $0.01^\circ$  ( $0.175 \, \text{mrad}$ ) using a belt drive (see label 5 in **Fig. 1**), without breaking the vacuum. This feature is foreseen in order to fine tune the orientation

<sup>6</sup> National Magnetics Group, Inc., Pennsylvania, USA, [http://www.magneticsgroup.com/m\\_ferr\\_nizn.htm](http://www.magneticsgroup.com/m_ferr_nizn.htm).

**Table 1**  
Operating frequencies  $f_{RF}$  of the waveguide RF Wien filter for deuterons ( $d$ ) at a momentum of 970 MeV/c and for protons ( $p$ ) at 520 MeV/c in COSY for the harmonic numbers  $k$ . The frequencies  $f_{RF}$  shown in bold fit in the frequency range from 100 kHz to 2 MHz. The revolution frequency  $f_{rev}$ ,  $G$  factors, Lorentz  $\beta$  and  $\gamma$ , and the spin tune  $\gamma G$  are given as well.

|     | $f_{rev}$ (kHz) | $G$    | $\beta$ | $\gamma$ | $\gamma G$ | $f_{RF}$ (kHz) |              |               |              |               |              |               |
|-----|-----------------|--------|---------|----------|------------|----------------|--------------|---------------|--------------|---------------|--------------|---------------|
|     |                 |        |         |          |            | $k = -4$       | $k = -3$     | $k = -2$      | $k = -1$     | $k = 0$       | $k = +1$     | $k = +2$      |
| $d$ | 750.2           | -0.143 | 0.459   | 1.126    | -0.161     | 3121.6         | 2371.4       | <b>1621.2</b> | <b>871.0</b> | <b>120.8</b>  | <b>629.4</b> | <b>1379.6</b> |
| $p$ | 791.6           | 1.793  | 0.485   | 1.143    | 2.050      | <b>1543.9</b>  | <b>752.2</b> | 39.4          | <b>831.0</b> | <b>1622.7</b> | 2414.3       | 3206.0        |

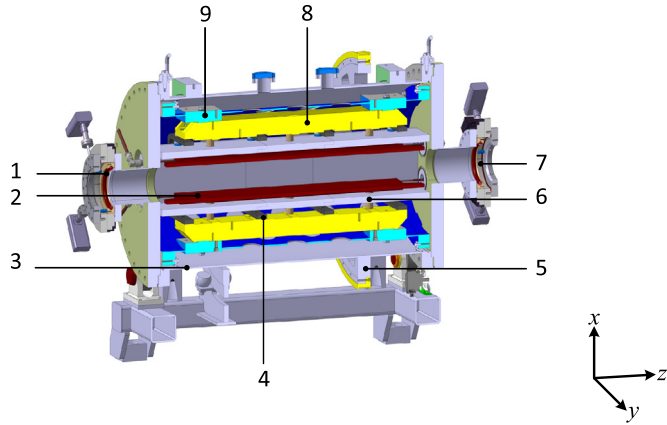


**Fig. 1.** Design model of the RF Wien filter showing the parallel-plates waveguide and the support structure. 1: Beam position monitor (BPM); 2: copper electrodes; 3: vacuum vessel; 4: clamps to hold the ferrite cage; 5: belt drive for 90° rotation, with a precision of 0.01° (0.17 mrad); 6: ferrite cage; 7: CF160 rotatable flange; 8: support structure of the electrodes; 9: inner support tube. The axis of the waveguide points along the  $z$ -direction, the plates are separated along  $x$ , and the plate width extends along  $y$ . During the EDM studies, the main field component  $E_x$  points radially outwards and  $H_y$  upwards with respect to the stored beam.

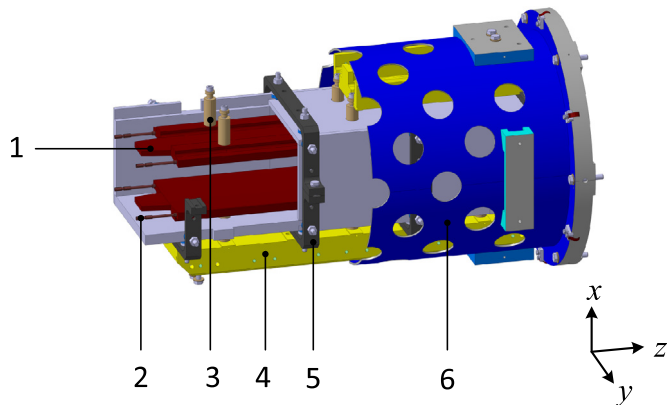


**Fig. 2.** Inner support structure of the RF Wien filter. 1: Copper electrodes with the trapezium shaping at the edges; 2: specially designed connector; 3: ceramic insulator between the electrodes and the support structure. A stainless-steel screw is located inside to connect the electrodes to the support structure; 4: support of the electrodes; 5: clamps to support the ferrite cage; 6: inner tube support structure.

of the RF Wien filter [12], and also to exchange the role of electric and magnetic fields during the EDM measurements for investigations of the systematics.

The parallel-plates waveguide constitutes a transmission line structure, which has been analyzed in detail in [19]. For the waveguide to be used as a Wien filter, wave mismatch must be introduced into the structure via a reflection, ensured by adding a resistor that controls the reflection coefficient. Thereby, the characteristic field quotient  $Z_q$ , given in Eq. (3), can be adjusted to the required value.

The multi-input feedthroughs ensure a homogeneous current distribution over the electrodes, the two parallel plates are connected to the amplifier and the load via four high-frequency, high-power CF 40 feedthroughs.<sup>7</sup> The electrodes are connected to the feedthroughs via specially designed connectors, and 3 dB power splitters are installed to feed each plate at the edges.

The RF Wien filter comprises a cage of ferrite blocks from CMD5005, which contains the electromagnetic fields within the Wien filter and enhances the field homogeneity. CMD5005 is a NiZn-type high-permeability ferrite material. Ref. [20] provides data of a dispersive model of the complex permeability  $\mu_r$  that have been used in the full-wave simulator at frequencies from 100 kHz to 2 MHz. At a frequency of 871 kHz, for instance,  $\mu_r = 1449 + i467$ . The relative permittivity  $\epsilon_r$  is around 25 [21]. CMD5005 elements come in blocks with a maximum length of 330 mm. The ferrites are held together by clamps in a symmetric arrangement. To make a connection between the electrodes and the main support structure possible, 12 boreholes are drilled in the ferrites. The screws supporting the electrodes are insulated from the ferrites by ceramic cylindrical insulators.

On each side of the CF100 entry and exit ports, 4 CF16 feedthroughs are connected for the beam position monitors (BPMs) [22], especially designed to ensure the alignment of the beam with respect to the axis of the RF Wien filter.

## 2.2. Driving circuit

Ideally, the driving circuit connects a load resistor directly to the electrodes, as shown in [19]. The amplifier (with 50  $\Omega$  internal impedance) is connected to the Wien filter via a (1:0.5) Balun [23] which transforms the impedance and converts the unbalanced output of the amplifier into a balanced one. A schematic of the driving circuit is shown in Fig. 3. One of the main characteristics of Balun transformers is their broadband response. The return loss  $L_r$  of the driving circuit (Fig. 3), calculated using CST Design Studio, is depicted in Fig. 4.

Another (1:1) Balun is used to connect the Wien filter to the load resistor. Introducing the cables into the schematic induces a phase shift between the electric and magnetic field, consequently, the field quotient  $Z_q$ , given in Eq. (3), becomes complex. This effect can be compensated with an additional inductance  $L_p = 8 \mu\text{H}$  (as indicated in Fig. 3), and an almost purely real-valued field quotient is obtained, i.e.,  $Z_q = 173 \angle 0.1^\circ \Omega$ .

## 2.3. Optimization of field homogeneity

For minimal Lorentz forces, the electric and magnetic forces must be matched at the center and the edges of the RF Wien filter. As mentioned before, the ratio between the electric and magnetic fields inside the RF Wien filter can be controlled via the load resistor  $R_m$ , and the inductance  $L_p$  (see Fig. 3). A special solution,

<sup>7</sup> VACOM Vakuum Komponenten & Messtechnik GmbH, Jena, Germany, <http://www.vacom.de>.

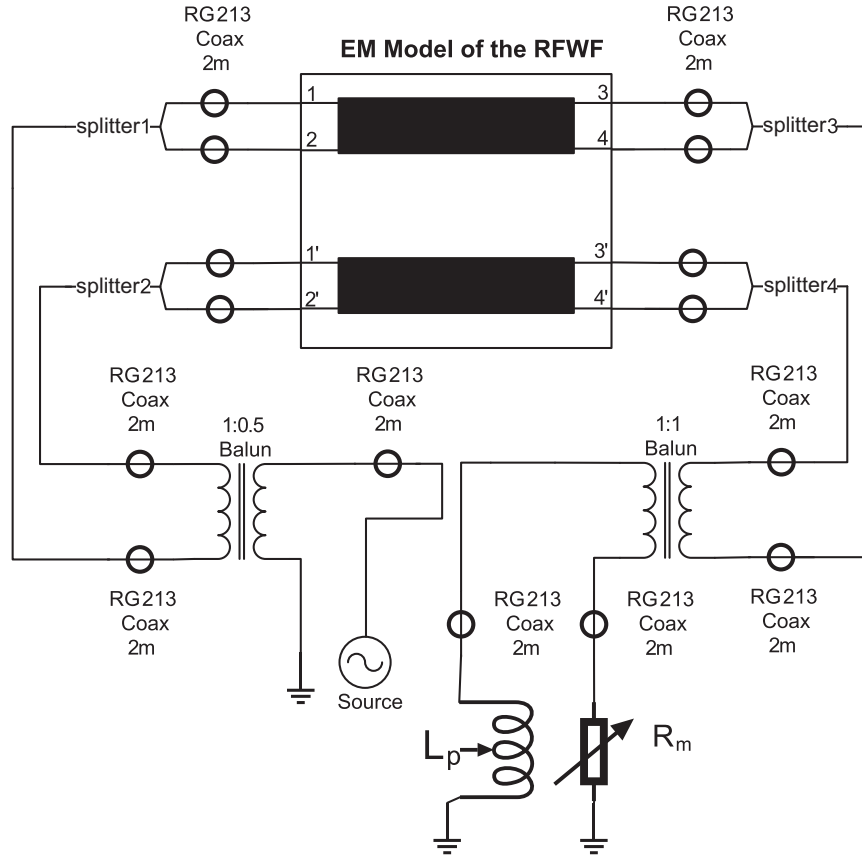


**Fig. 3.** Schematic of the driving circuit for the RF Wien filter. The condition for minimal Lorentz force is met using two adjustable devices, the resistor  $R_m$  and the inductance  $L_p$ .

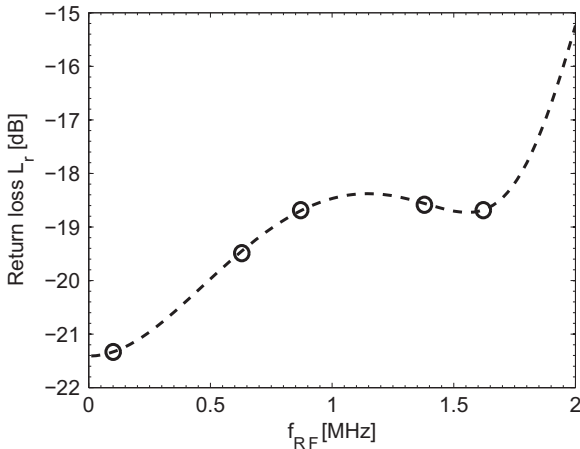


**Fig. 4.** Return loss  $L_r$  of the electromagnetic simulation of the circuit, shown Fig. 3. For the entire range of spin harmonics (from 0 to 2 MHz),  $L_r$  is below  $-15$  dB. Wideband matching is achieved with a 1:0.5 Balun.

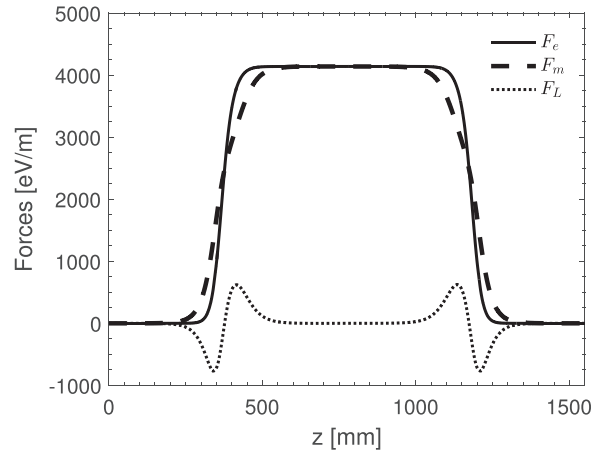


**Fig. 5.** Electric force  $F_e$ , magnetic force  $F_m$ , and Lorentz force  $F_L$  inside the RF Wien filter, for the geometry shown in Fig. 1. The integral Lorentz force is of the order of  $10^{-3}$  eV/m. The trapezoid-shaped electrodes at the entrance and exit of the RF Wien filter determine the crossing of electric and magnetic forces.

however, is required at the edges, where the slope of the curves of the electric and magnetic forces are not the same. According to our simulations, a simple parallel-plates waveguide deflects particles passing through the device in the same directions at the exit and entry points. Under these circumstances, the overall Lorentz force *cannot* be zero when the Lorentz force in the center is zero.

Our solution aims at a decomposition of the kicks at each side of the RF Wien filter into two deflections of opposite sign in such a way that both deflections average out. Decoupling the fields at the edges, keeping the electric field unchanged while manipulating the magnetic field, is accomplished by retaining the plate

separation (spacing between the plates), while altering the width of the plates [24]. In doing so, the slope of the curves of the electric field remains constant while the magnetic field crosses the electric field, as shown in Fig. 5. This approach results in trapezoid-shaped edges of the parallel plates, where the field crossing can now be optimized via the geometrical properties of the trapezoid-shaped edges. After performing a series of simulations, an optimum trapezoid depth of 50 mm, with a short base of 50.5 mm and a long base of 100 mm was found, as shown in Fig. 2 (label 1).

Integrating and averaging the Lorentz force  $\vec{F}_L$ , given in Eq. (2),

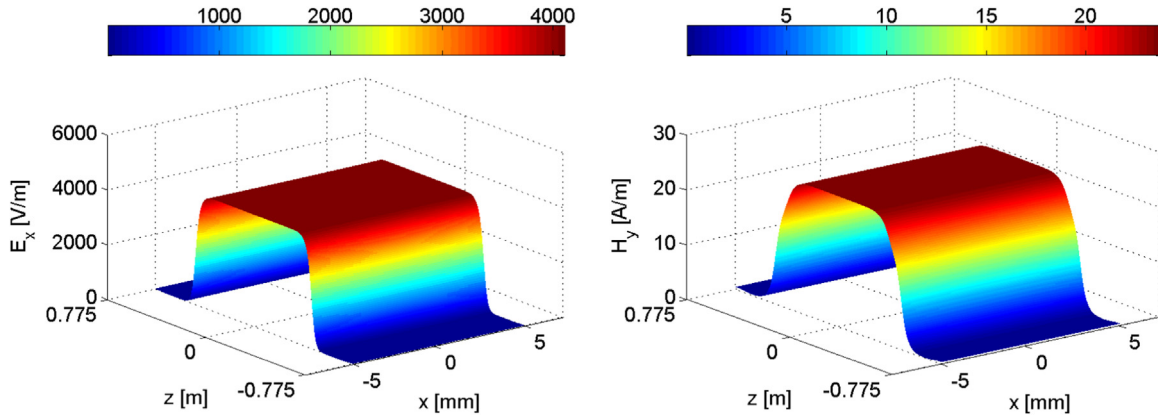


Fig. 6. Main components of the electric field  $E_x$  (left panel) and magnetic field  $H_y$  (right) of the waveguide RF Wien filter, for the geometry shown in Figs. 1 and 2.

along the axis of the RF Wien filter for the geometry shown in Fig. 1 at an input power of 1 kW, yields

$$\frac{q}{\ell} \int_{-\ell/2}^{\ell/2} \begin{pmatrix} E_x - c\beta B_y \\ E_y + c\beta B_x \\ E_z \end{pmatrix} dz = \begin{pmatrix} 5.97 \times 10^{-3} \\ 7.97 \times 10^{-3} \\ 1.27 \times 10^{-21} \end{pmatrix} \text{ (eV/m)}, \quad (4)$$

where  $\ell = 1550$  mm denotes the active length of the RF Wien filter, defined as the region where the fields are non-zero. The momentum variation in the beam of about  $\Delta p/p = 10^{-4}$  translates into a variation of the required field quotient  $Z_q$  of the same order of magnitude (see Eq. (3)), and therefore, the resulting values for the Lorentz forces, given in Eq. (4), are acceptable.

The waveguide RF Wien filter can be rated according to its ability to manipulate the spins of the stored particles, and as a figure of merit, the field integral of  $\vec{B}$  along the beam axis is evaluated, yielding for an input power of 1 kW,

$$\int_{-\ell/2}^{\ell/2} \vec{B} dz = \begin{pmatrix} 2.73 \times 10^{-9} \\ 2.72 \times 10^{-2} \\ 6.96 \times 10^{-7} \end{pmatrix} \text{ (T mm)}. \quad (5)$$

Under these conditions, the corresponding integrated electric field components are given by

$$\int_{-\ell/2}^{\ell/2} \vec{E} dz = \begin{pmatrix} 3324.577 \\ 0.018 \\ 0.006 \end{pmatrix} \text{ (V)}. \quad (6)$$

Fig. 6 shows the main (wanted) components of the electric and magnetic fields,  $E_x$  and  $B_y$ , in the  $xz$  plane.

In order to further increase the field homogeneity, the geometric parameters such as the width and the surface shape of the copper electrodes, and also the geometric parameters of the ferrite blocks and their distance to the metallic support structure, including the surrounding vacuum vessel were optimized.

The simulations showed that elliptically shaped electrode surfaces instead of flat ones substantially improve the local homogeneity of the electric field along the RF Wien filter. The parameters of the optimized elliptic electrodes are indicated in Fig. 7, with a major radius of 91 mm, and a minor radius of 6 mm, where the sharp edges have been rounded using a 1 mm radius. In the case of flat electrodes, the electric field varies up to 8 V/m, and by elliptically shaping the electrodes, as shown in Fig. 7, the electric field variation does not exceed 0.1 V/m.

The advantage of using elliptic electrodes is illustrated in Fig. 8, where the relative variation of  $E_x$  and  $H_y$ , e.g.,  $\left| \frac{E_x - \langle E_x \rangle}{E_x} \right|$ , is shown in the  $xy$  plane in the range  $x = \pm 5$  mm and  $y = \pm 5$  mm in the center of the RF Wien filter. The results are summarized in Table 2,

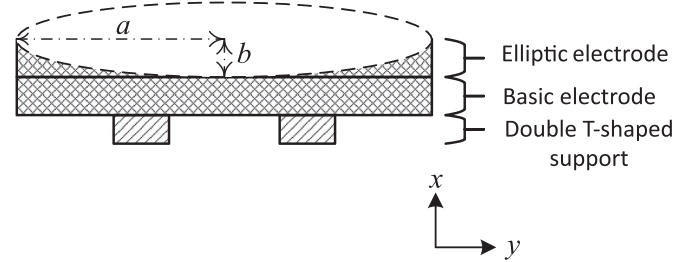


Fig. 7. Schematic view of the cross section of the bottom electrode. The double T-shaped support is used to fix the electrode to the support structure. The elliptic shape is constructed using an ellipse with a major radius of  $a = 91$  mm, and a minor radius of  $b = 6$  mm. Sharp edges are avoided using a rounding radius of 1 mm.

where the relative standard deviation of the data shown in panels (a), (b), (d), and (e) of Fig. 8 is listed. The elliptically shaped electrodes yield an improvement of up to a factor of 20 in terms of local electric field homogeneity while reducing the local homogeneity of the magnetic field by a factor of 11. In total, the Lorentz forces are about a factor 5 smaller for elliptically shaped electrodes with respect to flat-shaped electrodes.

### 3. Beam dynamics simulations

#### 3.1. Definition of unwanted field components

Due to the finite beam size, the beam particles are exposed to non-ideal field components of  $\vec{E}$  and  $\vec{H}$ . The system is designed such that *unwanted* field components average out at the exit and entry of the RF Wien filter. The unwanted field components are given by

$$\vec{E}_{\perp} = \begin{pmatrix} 0 \\ E_y \\ E_z \end{pmatrix} \quad \text{and} \quad \vec{H}_{\perp} = \begin{pmatrix} H_x \\ 0 \\ H_z \end{pmatrix}. \quad (7)$$

The index  $\perp$  is introduced to indicate that the unwanted electric and magnetic field components are perpendicular to the main field components  $E_x$  and  $H_y$ .

The particle beam that enters the RF Wien filter has a defined phase-space distribution [10], therefore the particles do not travel along straight lines, parallel to the beam axis. In order to quantify the effect of unwanted field components, a Monte-Carlo simulation based on solving the relativistic equation of motion using the time- and space-dependent fields has been carried out, with subsequent integration of the field components along the

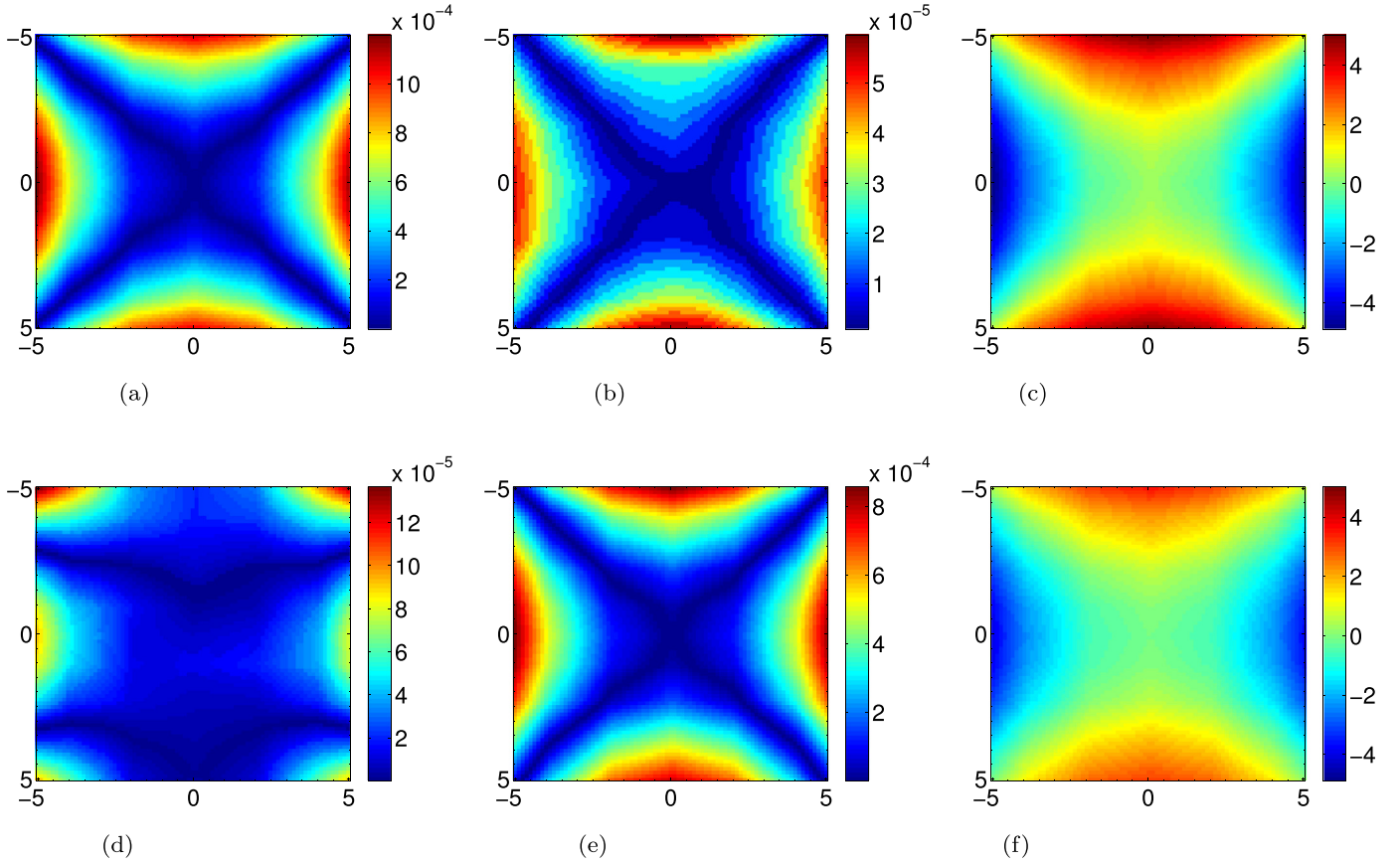


**Fig. 8.** Comparison of the field homogeneity of flat-shaped and elliptically haped electrodes across the beam extension in the range  $\pm x = 5$  mm and  $\pm y = 5$  mm around the beam axis in the center of the RF Wien filter ( $z=0$ ). The top row shows the fields variation of  $E_x$  (panel a) and  $H_y$  (b), and the Lorentz force (c) for flat-shaped electrodes, and the bottom row the corresponding results for elliptically-shaped electrodes,  $E_x$  (d),  $H_y$  (e), and the Lorentz force (f). (Note the different scale in the graphs.) (a) Flat:  $\left| \frac{|E_x| - \langle E_x \rangle}{|E_x|} \right|$ . (b) Flat:  $\left| \frac{|H_y| - \langle H_y \rangle}{|H_y|} \right|$ . (c) Flat: Lorentz force in eV/m. (d) Elliptic:  $\left| \frac{|E_x| - \langle E_x \rangle}{|E_x|} \right|$ . (e) Elliptic:  $\left| \frac{|H_y| - \langle H_y \rangle}{|H_y|} \right|$ . (f) Elliptic: Lorentz force in eV/m.

trajectories. The electromagnetic simulation yields the complex fields  $\vec{E}$  and  $\vec{H}$ . The real fields  $\vec{E}(\vec{r}, t)$  and  $\vec{H}(\vec{r}, t)$  are obtained from

$$\begin{aligned} \vec{E}(\vec{r}, t) &= \Re(\vec{E} e^{i\omega t}), \text{ and} \\ \vec{H}(\vec{r}, t) &= \Re(\vec{H} e^{i\omega t}). \end{aligned} \tag{8}$$

The relativistic equations of motion [25,26],

$$\begin{aligned} \frac{d\vec{v}}{dt} &= \frac{q}{m\gamma} \left[ \vec{E}(\vec{r}, t) + \vec{v} \times \vec{B}(\vec{r}, t) \right] \\ &\quad - \frac{q}{m\gamma c^2} \vec{v} \left[ \vec{v} \cdot \vec{E}(\vec{r}, t) \right], \text{ and} \\ \frac{d\vec{r}}{dt} &= \vec{v}, \end{aligned} \tag{9}$$

were solved in Matlab<sup>8</sup> using the field maps imported from the full-wave simulations. The mesh accuracy in the  $xy$  plane amounts to 0.1 mm and 11 mm in the  $z$ -direction. The phase-space distribution of the beam at the entry of the RF Wien filter is known [10]. The phase space is expressed in terms of positions  $x$  and  $y$ , and transverse angles  $x' = v_x/v_z$  and  $y' = v_y/v_z$ , respectively.

For each phase space, 5000 particles have been simulated with

**Table 2**

Calculated relative standard deviation (RSD) of the electric and magnetic fields in the cases of flat and elliptically shaped electrodes from Fig. 8, quantitatively indicating the achieved field homogeneity.

| RSD                                       | Flat shape            | Elliptic shape        |
|---|-----------------------|-----------------------|
| $\frac{\sigma(E_x)}{\langle E_x \rangle}$ | $4.74 \times 10^{-4}$ | $2.33 \times 10^{-5}$ |
| $\frac{\sigma(H_y)}{\langle H_y \rangle}$ | $3.17 \times 10^{-5}$ | $3.53 \times 10^{-4}$ |

a  $2\sigma$  beam emittance of  $\epsilon_{x,y} = 1 \mu\text{m}$ . The initial  $(x, x')$  phase-space distributions are shown in red in Fig. 9. The blue points represent the phase-space distribution of the particles after passing through the RF Wien filter. The  $(y, y')$  distributions are not shown, but are very similar. With low- $\beta$  section ON and OFF, the areas of the initial and final ellipses are the same, and consistent with the behavior of a field-free (drift) region. Thus the RF Wien filter does not appear to alter the phase-space distributions of the beam.

Based on the simulations, the effects of unwanted field components, given in Eq. (7), are quantified by integration along the particle trajectories, and expressed as ratios with respect to the total field integrals, yielding

$$f_{E_L}^{\text{int}} = \frac{\int i\vec{E}_L ds}{\int i\vec{E} ds}, \text{ and} \tag{10}$$

<sup>8</sup> Mathworks, Inc. Natick, Massachusetts, USA, <http://de.mathworks.com>.

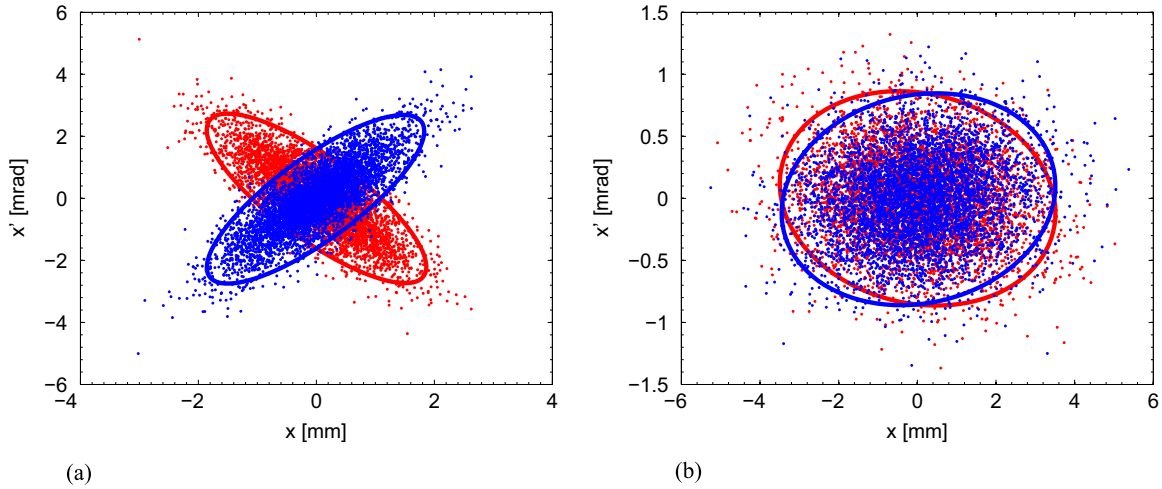


**Fig. 9.** Phase-space distributions ( $x, x'$ ) of a beam with an emittance of  $\epsilon_{x,y} = 1 \mu\text{m}$  entering (red) and exiting (blue) the RF Wien filter with low- $\beta$  section ON:  $\beta = 0.4 \text{ m}$  (panel a) and OFF:  $\beta = 4 \text{ m}$  (panel b). The ellipses show the  $2\sigma$  results of a fit with a 2D Gaussian distribution, respectively. (a) Low- $\beta$  section ON:  $\beta = 0.4 \text{ m}$ . (b) Low- $\beta$  section OFF:  $\beta = 4 \text{ m}$ . (For interpretation of the references to color in this figurecaption, the reader is referred to the web version of this paper.)

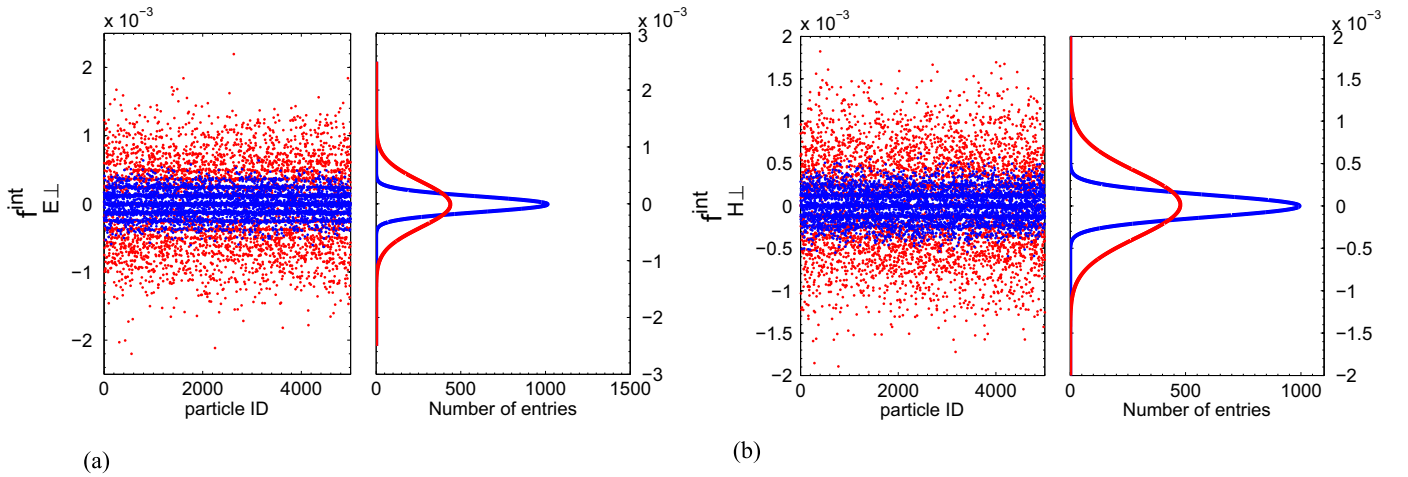


**Fig. 10.** Comparison of the unwanted electric (a) and magnetic (b) field components with low- $\beta$  section ON (red) and low- $\beta$  section OFF (blue). The right panels display Gaussian fits to the projections of the simulated distributions, respectively, summarized in Table 3. (a) Unwanted electric field components  $f_{E_{\perp}}^{\text{int}}$  from Eq. (10). (b) Unwanted magnetic field components  $f_{H_{\perp}}^{\text{int}}$  from Eq. (11). (For interpretation of the references to color in this figure caption, the reader is referred to the web version of this paper.)

$$f_{H_{\perp}}^{\text{int}} = \frac{\int |\vec{H}_{\perp}| ds}{\int |\vec{H}| ds}, \quad (11)$$

where  $ds$  denotes a differential element of the particle's path, which does not necessarily point along the  $z$  axis.

### 3.2. Results of beam dynamics simulations

The integrals in Eqs. (10) and (11) are evaluated for each of the 5000 simulated particles and for the two cases with low- $\beta$  section ON ( $\beta = 0.4 \text{ m}$ ) and OFF ( $\beta = 4 \text{ m}$ ). The results are shown in the left panels of Fig. 10, respectively, and summarized in Table 3. With low- $\beta$  section ON, the beam size is small, and the angular variation is large. As a consequence, the unwanted field components  $E_{\perp}$  and  $H_{\perp}$  do not completely cancel at the edges, leading to a wider distribution. When the low- $\beta$  section is OFF, the beam size is large, but with small angular spread, leading to a better cancellation of the unwanted field components at the edges.

The distributions in Fig. 10 exhibit a line structure that stems

from the finite mesh (0.1 mm in the  $xy$  plane, and 11 mm along  $z$ ). Gaussian fits to the projections of the resulting distributions  $f_{E_{\perp}}^{\text{int}}$  and  $f_{H_{\perp}}^{\text{int}}$  are shown in the right panels of Fig. 10, the fit results are summarized in Table 3. For the low- $\beta$  section either switched ON or OFF, the mean values of the integrated unwanted electric and magnetic field components are zero within the errors. The widths of the distributions, however, indicate that with low- $\beta$  section OFF, the unwanted electric and magnetic field components picked up by the beam are smaller by about a factor of two to three compared to when the low- $\beta$  section is ON. These findings should be further investigated using spin and particle tracking of a stored beam. In addition, once the device is installed, the predictions should be verified experimentally.

### 3.3. Comparison of prototype and waveguide RF Wien filter

The waveguide RF Wien filter is compared to the prototype RF Wien filter [16,17] (see Section 1) in terms of the unwanted field components, evaluated according to Eqs. (10) and (11), listed in Table 3. With the novel waveguide RF Wien filter, unwanted electric and magnetic field components can be reduced by one to

**Table 3**

Comparison of the prototype RF Wien filter [16,17] and the waveguide design in terms of unwanted field components  $f_{E_L}^{\text{int}}$  and  $f_{H_L}^{\text{int}}$  (see Eqs. (10) and (11)) using the simulated data, shown in Fig. 10.

| RF Wien filter |                  | $f_{E_L}^{\text{int}}$             |                      | $f_{H_L}^{\text{int}}$             |                      |
|----------------|------------------|------------------------------------|----------------------|------------------------------------|----------------------|
|                |                  | Mean $\mu$                         | Width $\sigma$       | Mean $\mu$                         | Width $\sigma$       |
| Waveguide      | Low- $\beta$ ON  | $(-1.1 \pm 0.8) \times 10^{-5}$    | $5.7 \times 10^{-4}$ | $(1.4 \pm 0.8) \times 10^{-5}$     | $5.5 \times 10^{-4}$ |
|                | Low- $\beta$ OFF | $(4.1 \pm 2.5) \times 10^{-6}$     | $1.8 \times 10^{-4}$ | $(0.8 \pm 2.6) \times 10^{-6}$     | $1.8 \times 10^{-4}$ |
| Prototype      |                  | $(1.454 \pm 0.009) \times 10^{-2}$ | $8.9 \times 10^{-3}$ | $(2.927 \pm 0.003) \times 10^{-2}$ | $3.0 \times 10^{-3}$ |

**Table 4**

Losses per material computed using the electromagnetic solver of CST Microwave Studio at a frequency  $f_{\text{RF}} = 1$  MHz.

| Material      | Thermal losses (mW) |
|---------------|---------------------|
| Copper plates | 95.7                |
| Ferrites      | 73.4                |
| Steel         | 25.5                |
| Ceramic       | 1.0                 |

two orders of magnitude.

Spin tracking simulation are required to quantify the systematic errors induced by unwanted field components, and by other systematic effects, e.g., positioning errors, and non-vanishing Lorentz forces in the determination of proton and deuteron EDMs.

#### 4. Thermal response of the RF Wien filter during operation

Because of the thermal insulation by the vacuum, we investigated whether even small power losses could lead to a temperature rise during operation. Therefore, for the corresponding thermal simulations using the FEM software ANSYS<sup>9</sup> only radiative heat exchange between the internal surfaces was considered. The entire power in the copper plates was assumed to be generated at the locations of the feedthroughs. The calculated power loss densities with an input power of 1 kW were integrated over the structural elements and are summarized in Table 4. The temperature rise for the copper electrodes is 6 K, and 0.5 K for the ferrites, respectively. Based on the temperature distribution, the simulated thermal expansion of the copper plates amounts to 48  $\mu\text{m}$ , and to 8.6  $\mu\text{m}$  for the ferrite blocks. These values are small compared to the dimensions of the structure, and we do not expect problems with respect to the electromagnetic performance and the suspension of the mechanical structure during operation of the RF Wien filter. In addition, the Lorentz force, given in Eq. (3), will be continuously minimized with a feedback system using a beam position monitor. Thus, during operation of the RF Wien filter the field quotient  $Z_q$  will be fine tuned using the resistor  $R_m$  and the inductance  $L_p$  in the driving circuit (see Fig. 3).

#### 5. Conclusion and outlook

This paper presents the electromagnetic design calculations for a novel type of RF Wien filter that shall be used at the COSY storage ring to determine the EDMs of deuterons and protons. The main emphasis of the work was to design a device that exhibits a

high level of homogeneity of the electric and magnetic fields. The optimization of the electromagnetic design was performed in close cooperation with the mechanical design, taking into account all the details of the mechanical construction.

A waveguide structure was selected because in this case the orthogonality of  $E$  and  $B$  fields, required for a Wien filter, can be ensured to a high level of precision. Minimizing the overall Lorentz force, while still providing sizable electric and magnetic field integrals, leads to elliptically-shaped electrodes, equipped with trapezoid-shaped entrance and exit partitions, surrounded by a closed box of ferrites. The corresponding profiles will be generated by CNC milling. Using the above described electrodes, the overall Lorentz force is reduced by about a factor of five, compared to flat-shaped electrodes.

The RF Wien filter will be installed in a section at COSY, where it is possible to vary the beam size by adjusting the  $\beta$  function between about  $\beta = 0.4$  and 4 m. Single-pass tracking calculations were performed in order to quantify the effect of unwanted electric and magnetic field components picked up by the beam, realistically distributed in phase space. The calculations indicate that unwanted field components picked up by the beam can be reduced by about a factor of three when the RF Wien filter is operated at  $\beta = 4$  m.

Thermal simulations show that the heat load in the different materials of the device, when operated with an input power of 1 kW is tolerable. Thus during operation, the mechanical accuracy of the device does not appear to substantially deteriorate the performance.

Forthcoming work will address improvements of the driving circuit, which will allow us to reach larger field values with the same input power. In addition, a novel semi-analytical approach to assess quantitatively the effect of mechanical tolerances on the electromagnetic performance of the RF Wien filter is presently being developed. By transversely displacing the beam inside the RF Wien filter, unwanted field components are picked up by the beam, leading to a departure from the situation with minimal Lorentz force. Thus, it will be possible to experimentally test the validity of tolerance estimates. Spin tracking studies are planned to quantify the impact of the waveguide RF Wien filter on the systematic error of the planned proton and deuteron EDM experiments.

#### Acknowledgments

This work has been performed in the framework of the JEDI (Jülich Electric Dipole Moment Investigations) collaboration. The authors would like to thank Martin Gaisser, Volker Hejny, Kirill Grigoryev, and Jörg Pretz for valuable comments on the manuscript.

<sup>9</sup> ANSYS, Inc. Canonsburg, USA <http://www.ansys.com>.



## References

- [1] F. Rathmann, A. Saleev, N.N. Nikolaev, The search for electric dipole moments of light ions in storage rings, *J. Phys. Conf. Ser.* 447 (2013) 012011, <http://dx.doi.org/10.1088/1742-6596/447/1/012011>.
- [2] W.M. Morse, Y.F. Orlov, Y.K. Semertzidis, RF Wien filter in an electric dipole moment storage ring: the partially frozen spin effect, *Phys. Rev. ST Accel. Beams* 16 (2013) 114001, <http://dx.doi.org/10.1103/PhysRevSTAB.16.114001>.
- [3] A. Riggio, M. Trodden, Recent progress in baryogenesis, *Annu. Rev. Nucl. Part. S* 49 (1) (1999) 35–75, <http://dx.doi.org/10.1146/annurev.nucl.49.1.35>.
- [4] W. Dekens, J. Vries, J. Bsaisou, W. Bernreuther, C. Hanhart, U.-G. Meißner, A. Nogga, A. Wirzba, Unraveling models of CP violation through electric dipole moments of light nuclei, *J. High Energy Phys.* 2014 7 (2014) 1–57, [http://dx.doi.org/10.1007/JHEP07\(2014\)069](http://dx.doi.org/10.1007/JHEP07(2014)069).
- [5] M. Salomaa, H. Enge, Velocity selector for heavy-ion separation, *Nucl. Instrum. Methods Phys. Res.* 145 (2) (1977) 279–282, [http://dx.doi.org/10.1016/0029-554X\(77\)90422-0](http://dx.doi.org/10.1016/0029-554X(77)90422-0).
- [6] G.H. Curtis, J. Silcox, Wien filter for use as an energy analyzer with an electron microscope, *Rev. Sci. Instrum.* 42 (5) (1971) 630–637, <http://dx.doi.org/10.1063/1.1685189>.
- [7] J. Orloff, *Handbook of Charged Particle Optics, Second Edition*, CRC Press, 2008.
- [8] B. Steiner, W. Ackermann, W. Mueller, T. Weiland, Wien filter as a spin rotator at low energy, in: Particle Accelerator Conference, 2007. PAC. IEEE, 2007, pp. 170–172, <http://dx.doi.org/10.1109/PAC.2007.4440148>.
- [9] R. Maier, Cooler synchrotron COSY - performance and perspectives, *Nucl. Instrum. Methods Phys. Res. A: Accel., Spectrometers, Detect. Assoc. Equip.* 390 (12) (1997) 1–8, [http://dx.doi.org/10.1016/S0168-9002\(97\)00324-0](http://dx.doi.org/10.1016/S0168-9002(97)00324-0).
- [10] C. Weidemann, et al., Toward polarized antiprotons: machine development for spin-filtering experiments, *Phys. Rev. ST Accel. Beams* 18 (2015) 020101, <http://dx.doi.org/10.1103/PhysRevSTAB.18.020101>.
- [11] M. Rosenthal, A. Lehrach, Spin tracking simulations towards electric dipole moment measurements at COSY, in: Proceedings, 6th International Particle Accelerator Conference (IPAC 2015), 2015, p. THPF032. (<http://accelconf.web.cern.ch/AccelConf/IPAC2015/papers/thpf032.pdf>).
- [12] S. Chekmenev, Estimation of systematic errors for deuteron electric dipole moment search at COSY, *Int. J. Mod. Phys. Conf. Ser.* 40 (2016) 1660099, <http://dx.doi.org/10.1142/S2010194516600995>.
- [13] M.A. Leonova, A.D. Krisch, V.S. Morozov, R.S. Raymond, V.K. Wong, R. Gebel, A. Lehrach, B. Lorentz, R. Maier, D. Prasuhn, A. Schnase, H. Stockhorst, D. Eversheim, F. Hinterberger, K. Ulbrich, Achieving 99.9proton spin-flip efficiency at higher energy with a small rf dipole, *Phys. Rev. Lett.* 93 (2004) 224801, <http://dx.doi.org/10.1103/PhysRevLett.93.224801>.
- [14] Spin-flipping crosses the Atlantic, *CERN Cour. Nov* 24, (<http://cerncourier.com/cws/article/cern/29208>).
- [15] S.Y. Lee, Spin resonance strength of a localized rf magnetic field, *Phys. Rev. ST Accel. Beams* 9 (2006) 074001, <http://dx.doi.org/10.1103/PhysRevSTAB.9.074001>.
- [16] S. Mey, R. Gebel, Towards an RF Wien-Filter for EDM Experiments at COSY, in: Proceedings, 6<sup>th</sup> International Particle Accelerator Conference (IPAC 2015), 2015, p. THPF031, (<http://accelconf.web.cern.ch/AccelConf/IPAC2015/papers/thpf031.pdf>).
- [17] S. Mey, R. Gebel, A Novel RF  $E \times B$  Spin Manipulator at COSY, *Int. J. Mod. Phys.: Conf. Ser.* 40 (2016) 1660094, <http://dx.doi.org/doi:10.1142/S2010194516600946>.
- [18] D. Eversmann, V. Hejny, F. Hinder, A. Kacharava, J. Pretz, F. Rathmann, M. Rosenthal, F. Trinkel, S. Andrianov, W. Augustyniak, Z. Bagdasarian, M. Bai, W. Bernreuther, S. Bertelli, M. Berz, J. Bsaisou, S. Chekmenev, D. Chiladze, G. Ciullo, M. Contalbrigo, J. de Vries, S. Dymov, R. Engels, F.M. Esser, O. Felden, M. Gaisser, R. Gebel, H. Glückler, F. Goldenbaum, K. Grigoryev, D. Grzonka, G. Guidoboni, C. Hanhart, D. Heberling, N. Hempelmann, J. Hetzel, R. Hipple, D. Hölscher, A. Ivanov, V. Kamerdzhiiev, B. Kamys, I. Keshelashvili, A. Khoukaz, I. Koop, H.-J. Krause, S. Krewald, A. Kulikov, A. Lehrach, P. Lenisa, N. Lomidze, B. Lorentz, P. Maanen, G. Macharashvili, A. Magiera, R. Maier, K. Makino, B. Mariański, D. Mchedlishvili, U.-G. Meißner, S. Mey, A. Nass, G. Natour, N. Nikolaev, M. Nioradze, A. Nogga, K. Nowakowski, A. Pesce, D. Prasuhn, J. Ritman, Z. Rudy, A. Saleev, Y. Semertzidis, Y. Senichev, V. Shmakova, A. Silenko, J. Slim, H. Soltner, A. Stahl, R. Stassen, M. Statera, E. Stephenson, H. Stockhorst, H. Straatmann, H. Ströher, M. Tabidze, R. Talman, P. Thömgren Engblom, A. Trzciński, Y. Valdau, E. Valetov, A. Vassiliev, C. Weidemann, C. Wilkin, A. Wirzba, A. Wrońska, P. Wüstner, M. Zakrzewska, P. Zuprański, D. Zyuzin, New method for a continuous determination of the spin tune in storage rings and implications for precision experiments, *Phys. Rev. Lett.* 115 (2015) 094801, <http://dx.doi.org/10.1103/PhysRevLett.115.094801>.
- [19] J. Slim, D. Heberling, Towards a high-accuracy RF Wien filter for spin manipulation at COSY Jülich, in: XVI International Workshop in Polarized Sources, Targets, and Polarimetry, 2015, p. PoS(PSTP2015)033.
- [20] H. Hahn, D. Davino, RHC abort kicker with reduced coupling impedance, in: Proceedings of the European Particle Accelerator Conference, EPAC, Paris, France, 2002, pp. 1502–1504, (<http://paper.kek.jp/e02/PAPERS/WEPRIO35.pdf>).
- [21] S.Y. Zhang, Resonance Model of Ferrite Assembly for Window Frame Magnet Kicker Impedance, 2000, <http://dx.doi.org/10.2172/1061616>.
- [22] F. Hinder, Development of new beam position monitors at COSY, in: Proceedings of the International Beam Instrumentation Conference, IBIC2015, Melbourne, Australia, 2015, Submitted for publication (<http://ibic.synchrotron.org.au/papers/tupb015.pdf>).
- [23] I. Hickman, *Practical RF Handbook*, EDN Series for Design Engineers, Elsevier Science, 2006.
- [24] D. Pozar, *Microwave Engineering*, Wiley, 2004.
- [25] S. Humphries, *Charged Particle Beams*, Dover Publications, 2013.
- [26] H. Wiedemann, *Particle Accelerator Physics, Graduate Texts in Physics*, Springer International Publishing, 2015.